Arch. Metall. Mater. **66** (2021), 3, 831-838

DOI: 10.24425/amm.2021.136387

G. SELVAKUMAR[1], S. RAM PRAKASH[1*], K. RAJKUMAR[1]

EVALUATION OF THE MECHANICAL AND ELECTRICAL PROPERTIES OF SPARK PLASMA SINTERED TITANIUM CARBIDE REINFORCED ALUMINA CERAMIC COMPOSITE

Spark Plasma Sintering (SPS) is identified as a suitable technique to prepare the alumina titanium carbide composite to overcome the difficulty in fabricating it through other consolidation method. The present work focuses on the fabrication and characterization of a series of titanium carbide reinforced alumina ceramic composites using a spark plasma sintering process. The titanium carbide reinforcement on the alumina matrix is varied between 20 and 35 wt.%, in order to improve the electrical conductivity and fracture toughness of the composites. The particle size of the starting powders at received and ball milled conditions was analysed through Particle size analyser and Scanning Electron Microscope (SEM). Microstructural analysis revealed that the TiC reinforcement is uniformly dispersed in the sintered composite. XRD report showed that α-alumina and titanium carbide were the two dominant phases without the formation of any reaction phases. Further, the correlation between mechanical and physical properties of the prepared composite was investigated as a function of TiC. Various fracture toughening indicators like crack deflection, bridging and branching were analysed by Vicker's indentation method. Electrical resistivity of the sintered compact decreases proportionally with the increase in titanium carbide constituents. Maximum density (98.80%) and hardness (20.56 GPa) was obtained for 30 wt. % reinforced composite. Almost 40% improvement in fracture toughness is noted for 25 wt. % reinforced composite. This work demonstrates the synthesis and fabrication of alumina titanium carbide composites at low temperature via SPS resulted in obtaining an intact compact with improved mechanical and electrical properties.

Keywords: Spark Plasma Sintering, Alumina composite, TiC, Mechanical properties, Fracture toughness

1. Introduction

Alumina is the promising and highly sought-after material predominantly used for metal cutting tools, vacuum process chambers, hip plants, semiconductor devices, liquid crystal displays and microwave absorbing materials due to its thermal stability, high hardness, high refractoriness, excellent corrosion and wear resistance [1-3]. Moreover, alumina having the grain size less than 1μm and relative density of about 99.95% has the tendency of being transparent. Unlike other materials, alumina with cubic structures acts as birefringent [4]. Inherently, alumina has low toughness and fracture strength that limits the horizon of its development and applications. Amidst the eight distinct crystal structures of alumina, α-alumina is well known for its stability, and calcinating other phases at high temperatures (above 1000°C). It also possesses excellent chemical and thermal properties. Nevertheless, the sinterability of alumina composite poses a great challenge in the synthesis and processing stages to achieve a highly densified composite. Low self-diffusion coefficient and high melting point of alumina leads to high sintering temperature. Alternate approach is appending carbide and boride particles in the form of whiskers or particles to enhance the sinterability of the process. Previous literatures reported that the addition of SiC [5], BC [6], and NbC [7] will drastically improve the mechanical properties in some cases which is likely due to the solid solution formation during compaction. Further, it may reduce the sintering temperature and ease the mass diffusion.

Titanium carbide (TiC) possessing strong covalent bond, preferred as suitable reinforcement material because of its superior properties like high melting point, excellent thermal and electrical conductivity, and good wear resistance [8-11]. It is invariably used for metal working tools, fuel cell, nuclear reactor and high temperature applications like turbine blade. Addition of TiC impedes the starting materials grain growth and likely to improve the mechanical properties and densification behaviour [12,13]. Increase in TiC concentration improves the electrical conductivity of the composite that leverages the utility of the material in various avenues [14].

[1] DEPARTMENT OF MECHANICAL ENGINEERING, SRI SIVASUBRAMANIYA NADAR COLLEGE OF ENGINEERING, CHENNAI, INDIA

* Corresponding author: ramprakashnec@gmail.com

Densification of composite material at minimal temperature with ultra-fine microstructure is of special interest pertaining to the enhancement of mechanical property. It is obvious that the microstructural refinement is attained by employing sophisticated sintering techniques. Common sintering methods lead to abnormal grain growth, high porosity, environmental problems, low purity, and longer dwell time [15]. Nonetheless, it results in poor mechanical properties like low flexural strength and toughness. The grain size of both the matrix and reinforcement is to be controlled to enhance the hardness and toughness of the materials. Hence, selection of sintering technique is indeed crucial for attaining microstructural refinement and to promote rapid densification.

Spark Plasma Sintering (SPS) process is a novel solid state sintering technology that synergize the effect of pulsed DC electric current and uniaxial force, to diffuse the powder particles by heating [16]. Sintering kinetics of SPS is greatly improved by electric field assisted particle diffusion, and internal localized joules heating between the particles [17-20]. Generally, it is a robust and one-step densification process operated with shorter production cycles. Unlike other methods, it is likely to operate with a high heating rate, fast and uniform compaction that leads to high densification and low grain growth [21,22]. It is a well-established and effective method for sintering ceramic and refractory materials. It is speculated that the spark discharges emanated during sintering in SPS. Based on that propositions, the generated spark discharges have the potential to clean the particle surface and tends to produce favourable current flow in between the particles. The newly formed electrical pathway assists in direct heating of the powders while sintering by Joule's effect.

This cutting edge technology tends to mitigate the grain growth as it produces internal localized heat on the particle surface by selecting the appropriate conditions like pressure, temperature and holding time [16,19,23]. Hence, SPS is identified as the potential candidate to process high temperature ceramics. It has the process capability with the heating rate of 1000°C per minute. The absence of any insulating system inside the water cooled cabinet and low thermal inertia of the system drastically reduce the whole thermal cycle. Besides processing the conductive materials, it also has the ability to densify insulating materials [24]

Nonetheless, many researchers discussed the sintering behaviour, densification, toughening agents, physical and mechanical properties of the TiC reinforced alumina ceramics through common sintering technique like pressureless sintering, hot pressing, and microwave sintering [25-28]. This particular research work intent to employ advanced sintering techniques like SPS to fabricate alumina matrix composites reinforced with different compositions of TiC (20,25,30 and 35 wt. %). The effects of TiC on the hardness, fracture toughness, and electrical conductivity of the alumina composite have been investigated. Phase constituents of the sintered composite is evaluated by conducting XRD test. SEM micrographs reveal the microstructure of the powder and sintered composite.

2. Materials and methods

In this study, α-Alumina (Sigma Aldrich – 99.5% purity), and Titanium Carbide (Sigma Aldrich – 99% purity) were chosen as the starting materials. The starting powders were separately ball milled with zirconia and tungsten carbide balls to reduce the particle size in the planetary ball mill. The ball to powder ratio is taken as 10:1. The planetary ball mill is allowed to rotate with 250 rpm for 7 hours in dry condition [29]. The particle size of the received and milled powders was measured by particle size analyser (Model: HORIBA, LA-950). The experimental pattern for fabricating alumina titanium carbide composites is presented in Fig. 1. The milled powders of alumina and TiC were blended stoichiometrically. After blending, the pulverized particles were loaded in a graphite die for compaction. Inside the SPS chamber (DR. SINTER, SPS-625 Syntex Incorporation, Japan) the graph-

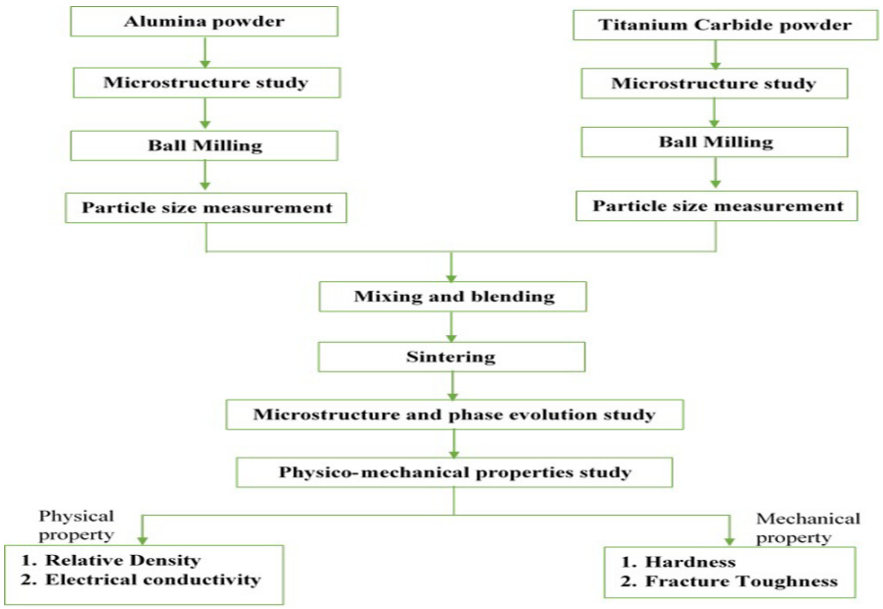

Fig. 1. Line diagram for the fabrication of alumina titanium carbide composite

ite die and plunger setup was placed between the electrodes and arranged with aid of spacers under vacuum conditions. Fig. 2. represents the photographic image of sintering experimentation. In SPS process, the partial pressure and sintering atmosphere plays a significant role on the diffusivity of the sintering material. There are several other phenomena like sintering kinetics, grain growth, phase stability, and stoichiometry are greatly influenced by the sintering environment [30]. Adsorption of gas, water or organics tends to reduce the surface energy of the particles which deteriorates the thermodynamic driving force and sintering. In general, the sintering in CO_2 atmosphere inhibits the diffusion of particles due to the formation of carbonate layers. Sometimes, the gas entrapped in the compact restricts the full densification. The inner side of the die wall was wrapped with thin graphite sheet to facilitate the ejection of the compact after sintering process. The temperature of the graphite die inside the chamber was monitored by using an optical pyrometer. The following sintering conditions were observed for the fabrication of alumina and TiC composite such as temperature = 1450°C, uniaxial pressure = 40 MPa, holding time = 5 min, heating rate = 100°C per minute. The density of the prepared sample was computed by Archimedes principle. The relative density (RD) of the compact was calculated by considering the ratio of actual density to theoretical density. The phase evolution and grain structure of the compact after sintering were identified by XRD (Malvern Panalytical, Empyrean) analyses using Cu as target for the wavelength $\lambda = 1.54$ Å, 2 theta in the range of 10° to 80° with the scan rate of 0.02°. The resistivity of the sample is measured using Agilent 34401A 6½ Digital Multimeter [31]. The sintered compact was grounded with SiC papers up to #2500 followed by diamond paste polishing. The microstructure of the sintered samples was observed under FESEM (Carl Zeiss, Sigma). Vickers micro hardness (H_V) (Wilson Wolpert – Germany) of the polished samples was measured under the applied load of 5 N and dwell time of 10 seconds.

The Vickers hardness value of the sintered compact was derived by the below equation [32]

$$\mathrm{Hv} = 0.1891\frac{F}{d^2} \tag{1}$$

Where F and d represents the indentation load and diagonal length of the indent.

Vickers Indentation Fracture (VIF) is the simplest, accurate, and common method to measure the toughness of the bulk material. Further, the fracture toughness was computed by the following equation [17],

$$K_c = 0.016\left(\frac{E}{\mathrm{Hv}}\right)^{\frac{1}{2}}\frac{P}{C^{\frac{3}{2}}} \tag{2}$$

Where E represents the Young's modulus calculated by rule of mixtures, Hv indicates the Vickers hardness value, P is the applied load and C represents the average of half crack length.

3. Results and discussion

3.1. Microstructure characterisation of received and ball milled alumina and TiC

The microstructure of alumina and titanium carbide powder in as-received and milled conditions were presented in Fig. 3 and Fig. 4. Both alumina and TiC grains are angular and existed in different size ranges. These figures exhibit different particle shape and size after ball milling. A highly dense ceramic structure is obtained by the irregular particle shape and size that greatly influences the mechanical properties [33]. Table 1 presents the average particle size of the starting powders in as-received and ball milled condition. The size of the alumina powder is reduced

Fig. 2. Photosnap of the SPS machine and prepared composite

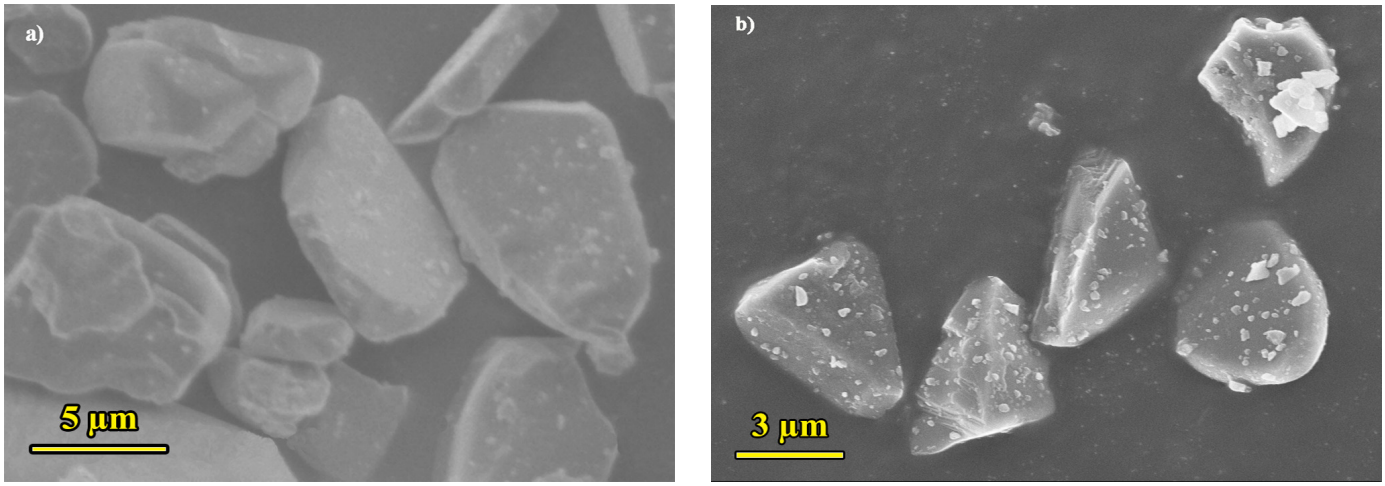

Fig. 3. Alumina powder a) as received and b) milled condition

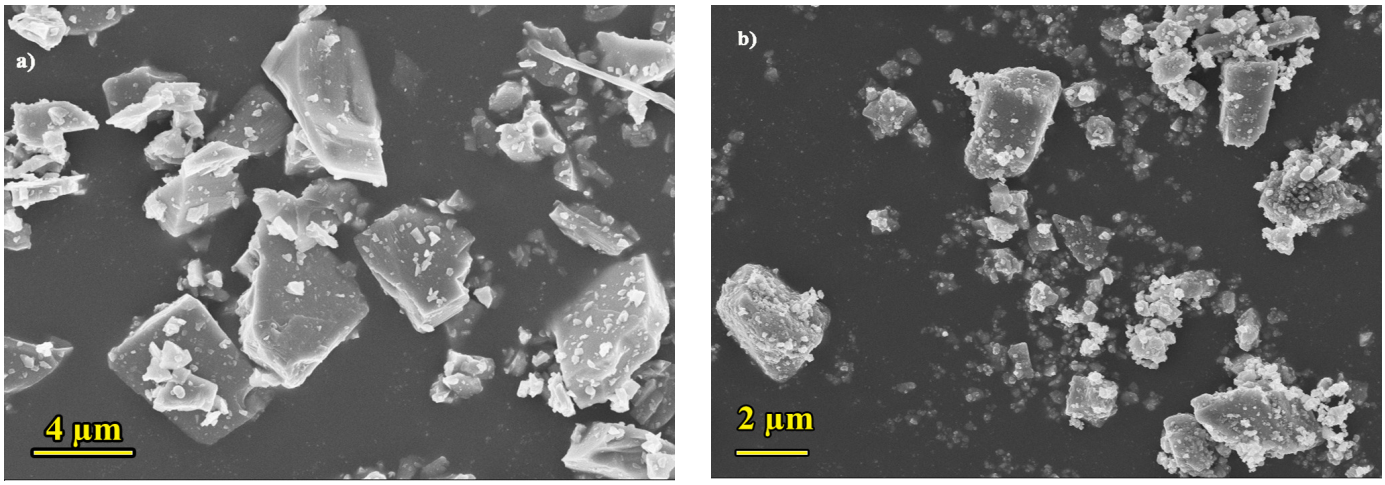

Fig. 4. Titanium carbide powder a) as received, and b) milled condition

to half of its initial form whereas the TiC is reduced to one-fourth of its actual size. Singh et al. [34] reported that the milled powder increases the specific surface area and contact points between the particles which in turn enhances the sintering kinematics.

TABLE 1

Particle size of powders

Material	Received powder size (µm)	Milled powder size (µm)
Al_2O_3	10.26 ± 1.87	5.32 ± 1.66
TiC	4.15 ± 1.28	1.39 ± 0.55

3.2. EDS analysis and microstructure investigations of the sintered samples

EDS analysis performed at the cross section of the sintered sample to evaluate its chemical composition. The elemental composition of the sintered composite for 25 wt. % is shown in Fig. 5. The FESEM images of the sintered composite with varying TiC reinforcement is shown in Fig. 6. From the FESEM micrographs, TiC and Al_2O_3 are easily distinguishable and identified as the white and the grey particles [35]. Moreover, it is evident from the SEM micrograph that the good metallurgical joint was established in the alumina and TiC interface. The interface between the matrix and the reinforcement could be crucial on deciding the mechanical properties [36]. The TiC particles embedded in the alumina matrix became spheroidal that confirms the partial dissolution of TiC in alumina during sintering. As can be seen in the Fig. 6(a-d), the reinforcement particles are homogenously distributed throughout the alumina matrix excluding 35 wt. %. In Fig. 6(a), drop off traces were noticed on some localized areas of the composite that is due to the surface grinding using sand paper, and few micro-cracks were also observed. Fig. 6(b-d) shows some random occurrence of porous structure in the sintered compact.

3.3. Phase evolution of powder and consolidated samples

The diffraction peak pattern for the alumina and TiC powder in received and milled condition were illustrated in Fig. 7(a, b). It is interesting to note from Fig. 7(b) that the milled

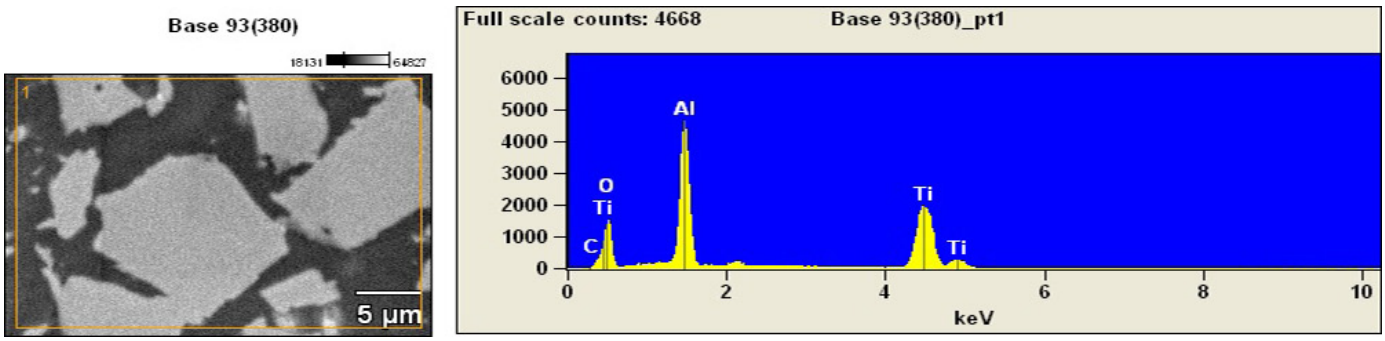

Fig. 5. EDS analysis of Alumina – 25 wt. % TiC composite

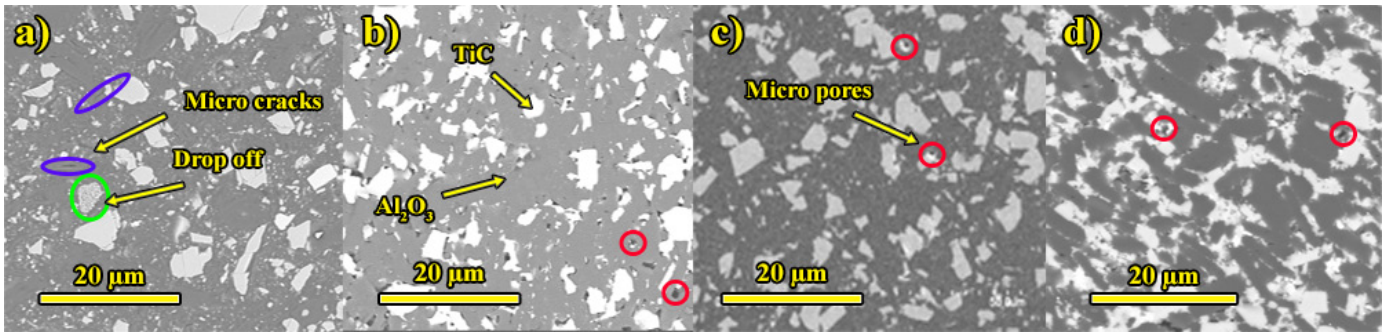

Fig. 6. FESEM of the composites a) 20% b) 25% c) 30% d) 35% TiC

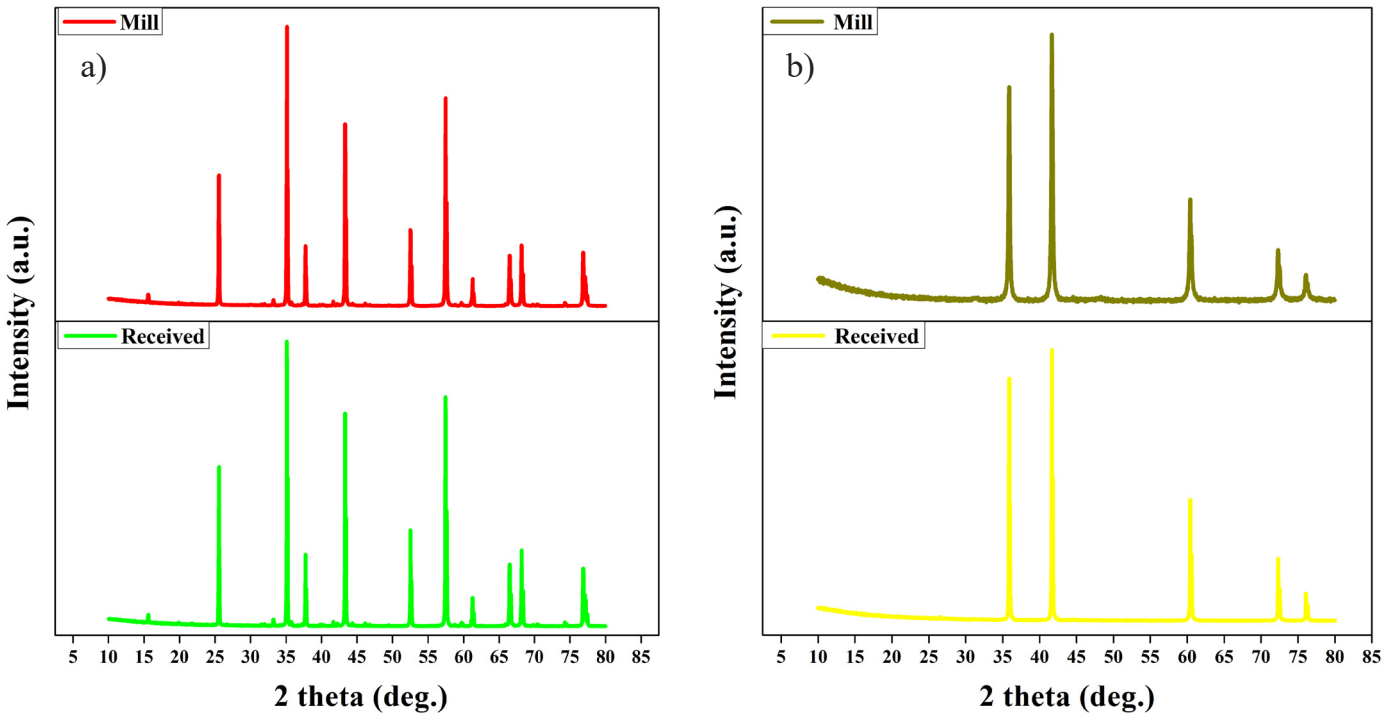

Fig. 7. XRD pattern of powders in received and milled condition a) Alumina b) Titanium carbide

TiC peak is quite broaden in comparison with the received powder. Akbarpour et al. [37] reported that the crystal size of the particle decreases proportionally with the broadening of peak, as per Williamson – Hall plot formula. The peak broadening with less intensity suggests decrease in particle size and increase in lattice strain during ball milling [38]. Owing to the great impact of balls on the alumina and TiC particles causes fracture during ball milling process. This effect escalates the defect density especially the dislocation that reduces the particle size. Thus, it confirms the considerable reduction in TiC particle size after ball milling and no remarkable change is observed in the alumina peak pattern.

The XRD spectrum of the sintered composites with respect to TiC constituents is presented in Fig. 8. It is revealed that the diffraction peak of TiC gradually rises with increase in the TiC content. From the XRD spectrum, the phases and their unit cell of major elements of the sintered compacts were detected as α phase – alumina and titanium carbide. This is done by matching the obtained data with JCPDS file no. 811667 and 893828. Thus, both α – alumina and titanium carbide observed to be rhombo-centered and face centered cubic structure respectively. Both the matrix and the reinforcement does not involve in any additional reaction to form any by-products. Hence, it is evident to conclude that the sintered composites were successfully fabricated with the desired phase constituents. However, some asymmetric peaks pattern was seen for the TiC peaks, especially found on 30 and 35 wt. %. The prime reason for the occurrence of non-symmetric peak pattern is due to the stacking fault, distortion, concentration rate, and strain [39].

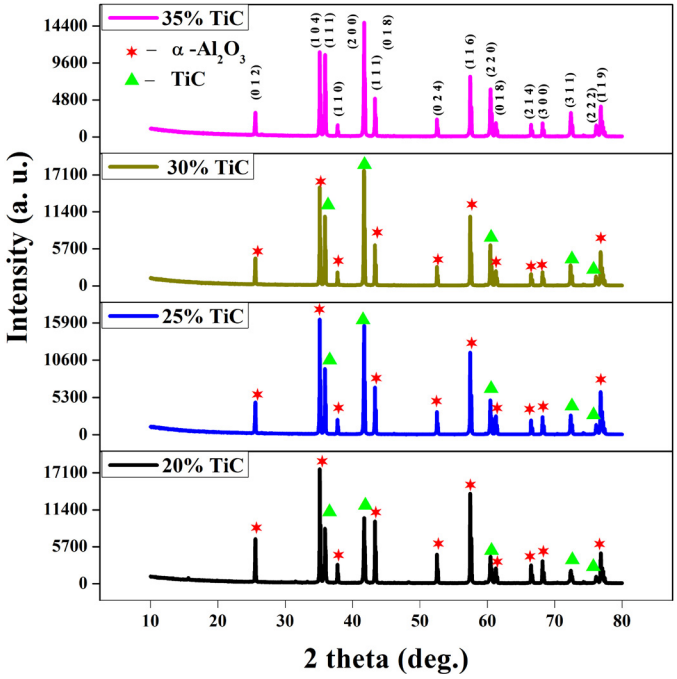

Fig. 8. XRD patterns of fabricated Alumina – TiC composites

3.4. Electrical resistivity of the sintered composite

Fig. 9 presents the electrical resistivity of the sintered samples with varying TiC concentrations. It exhibits that there is a rapid decrease in the resistivity of the sample with the addition of TiC. The obtained results are in concurrence with the findings of Wang et al. [2]. Amongst all the compositions, 30 and 35 wt. % are likely to act like low conductive material, and shows better prospects to be processed through thermo-electric process by adopting suitable strategy. Inspite of its moderate electrical behaviour it can be viable to utilize these composites in energy storage devices and microwave absorbers at elevated temperature conditions. Zhang et al. [40] stated that the alumina (70%) + TiC (30%) can be opted for magnetic disk drives due to its sort of metal like conductivity that can be helpful in dissipating the charge accumulation during frictional contact.

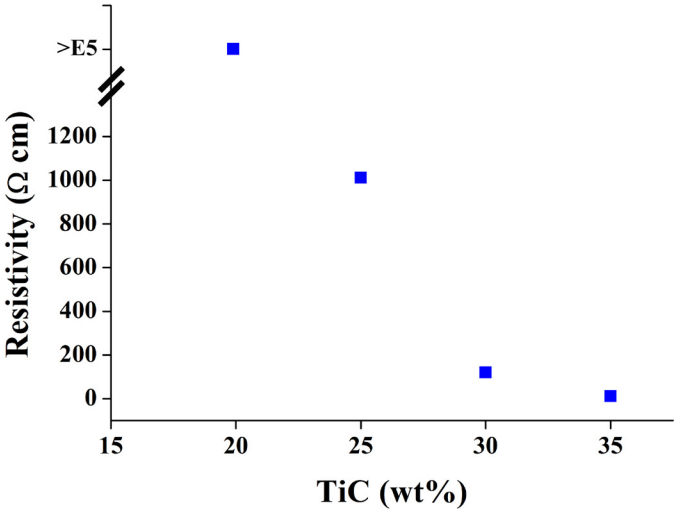

Fig. 9. Resistivity of the composite as a function of TiC

3.5. Physicomechanical properties of bulk samples

Table 2 reports the relative density, Vickers hardness, fracture toughness of the sintered composites. The sample constitutes of 30 and 35 wt. % has been fairly sintered with the density above 98%. The results revealed that the increase in TiC concentration accelerates the sintering behaviour to achieve better densification. In contrast, the sample with lesser TiC constituents like 20 and 25 wt. % exhibits lesser densification due to higher electrical resistivity. In SPS, the heat generation required for grain boundary migration and matter transport during sintering were controlled by the electrical resistance of the die and the powder constituents [30]. Langer et al., [41] and Babapoor et al., [42] elucidated that the applied electric current along with electrically conductive particles acts as the drive force for quick densification at relatively low temperature. In case of sintering conductive media, it is presumed that the spark discharges evoked in the gap between the grains leads to localized heat generation. This effect is further assisted by Joule's law of heating forming a thermal runway resulted in rapid densification [43]. Hence, it is observed that the change in electrical resistivity of the sample influences the current path way and temperature evolution.

TABLE 2

Physical and mechanical properties of the SPS sintered composites

S. No.	Al_2O_3 (wt%)	TiC (wt%)	Relative Density (%)	Micro hardness (GPa)	Fracture toughness MPa $m^{½}$
1.	80	20	87.07	7.728 ± 0.3	2.16 ± 0.4
2.	75	25	93.87	8.933 ± 0.1	3.01 ± 0.5
3.	70	30	98.80	20.56 ± 1.49	2.45 ± 0.3
4.	65	35	98.63	14.16 ± 1.3	2.26 ± 0.6

Like relative density, the hardness also follows the same trend as it is attributed to density of the composite. The obtained results stated that the hardness of the sintered compact is increased by adding TiC particles. The maximum hardness of 20.56 GPa is achieved for 30 wt. % for the operating conditions of 1450°C and 40 MPa. It is seen that SPS sintering increased relative density by 1.3% and hardness by 18% when compared with hot-pressed alumina-TiC composite [26]. However, more TiC (35 wt. %) concentration leads to the conglomeration of particles, which decreases the hardness of the composite. It is inevitable to control the particle agglomeration when bidding for higher stoichiometry ratio, and this acts an impedance on achieving desired mechanical properties [1,44]. Namini et al. [13] reported that the composite hardness depends on various phenomenon like stoichiometry, grain growth, particle shape [41] and relative density.

The fracture toughness of the sample is examined with VIF method at higher loading conditions to witness a well-developed crack on the indentation tip. The total crack length (indentation centre to the crack tip) was measured by using SEM micrographs. The indentation load was set as 500 N for all the sintered compacts to measure the fracture toughness. At this condition, radial cracking was observed at the corners of the indent. Table 2 presents the fracture toughness of the sintered compact. An increasing trend in fracture toughness is observed till 25 wt. % afterwards, it exhibits the reverse trend. No remarkable improvement is noticed in fracture toughness of the composite regardless of the TiC addition. The same observations were reported by Tuzemen et al. [8], where the addition of TiC in titanium based molybdenum alloy significantly decreased the fracture toughness of the composite.

Fig. 10 reports the SEM micrographs of the polished surface indicating the crack propagation behaviour of the sintered compact for 30 wt. %. In Fig. 10(a-c) several toughening agents like crack deflection, crack branching and crack bridging were observed. Fig. 10(a) explicitly reveals the crack deflection mechanism of the compact. It is interesting to note that the cracks were deflected from its side as it advances the TiC particles and passes through the interphase of the particles evidencing intergranular mode of fracture. This effect is due to the institution of residual strain between the matrix-reinforcement interface. The onset of residual strain resulted in colossal variations in the coefficient of thermal expansion of the matrix-reinforcement phases that led to weak interfaces. This phenomenon affects the indigenous property of the material but enhances the toughening mechanism via extensive crack propagation. Mismatch in the crystallographic structure and particle orientation defines the crack deflection mechanism. Further, it is intensively improved by the incorporation of reinforcement with different crystal structure and material property. Crack bridging mechanism is rarely observed on some sites of the compact which is presented in Fig. 10(b). Besides, the crack branch mechanism is exhibited in Fig. 10(c) where the branching of the crack initiates at the indentation tip of the sintered compact. In this mechanism, the total energy of the crack is parted into multiple cracks that can be tolerated by the microstructure of the sample which acts as an additional impetus for the improvement in fracture toughness.

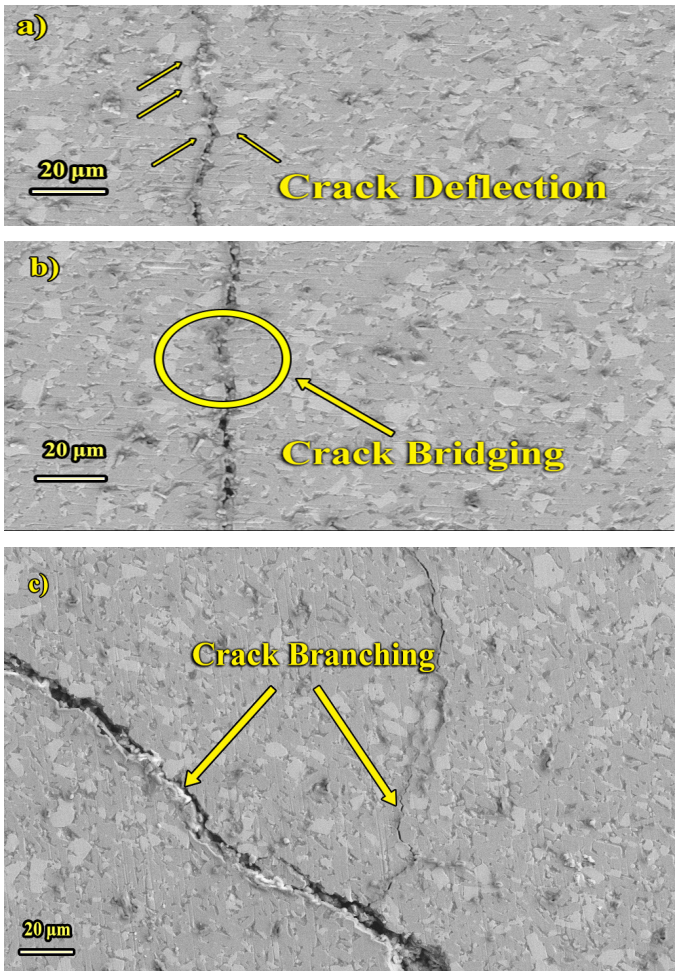

Fig. 10. SEM images of micro indentation crack indicating various fracture mode for 30 wt. % TiC a) crack deflection b) crack bridging c) crack branching

4. Conclusions

Titanium carbide reinforced alumina ceramic composite with varying compositions of TiC have been successfully fabricated through SPS technique. The prepared composites can be viable to use in cutting tool industry, disk drive companies and energy storage products because of their mechanical and electrical applications. Microstructure characterization of the matrix and reinforcement particles before and after ball milling were investigated. XRD pattern manifests that the sintered composites were fabricated with the desired constituents without any reaction products at this sintered conditions (temperature – 1450°C). The homogenous dispersion of TiC particle in the sintered composite is evident from the SEM micrographs except 35 wt. %. The chemical composition of the prepared composite is verified by conducting EDS analysis. The addition of TiC particle in the alumina matrix drastically reduces the electrical resistivity of the composite. The maximum relative density (98.80%) and hardness (20.56 GPa) is achieved for the 30 wt. % composite.

No significant improvement in the fracture toughness value is observed regardless of its reinforcement compositions. Crack deflection, branching and bridging were detected as the toughening mechanisms from the vickers indentations.

Acknowledgments

The authors acknowledge and thank the Department of Science Technology – Science and Engineering Research Board (DST – SERB), India [Grant No: ECR/2016/001517] for their financial support and extended thanks to Dr. S.R. Koteswara Rao, Professor and Head, Mechanical department, Sri Sivasubramaniya Nadar college of engineering, Dr. B. S. Murthy, Director, IIT Hyderabad and Dr. Dibyendu Chakravarty, Scientist – E, ARCI, Hyderabad for their moral support.

REFERENCES

[1] Y. Tamura, B.M. Moshtaghioun, D.G. Garcia, A.D. Rodriguez, Ceram. Int. **43**, 658-663 (2017).

[2] Y. Wang, F. Luo, W. Zhou, D. Zhu, J. Electron. Mater. **46** (8), 5225-5231 (2017).

[3] G.M. Asmelash, O. Mamat, F. Ahmad, A.K.P. Rao, J. Adv. Ceram. **4** (3), 190-198 (2015).

[4] S. Ghanizadeh, S. Grasso, P. Ramanujam, B. Vaidhyanathan, J. Binner, P. Brown, J. Goldwasser, Ceram. Int. **43**, 275-281 (2017).

[5] E.S. Gevorkyan, M. Rucki, A.A. Kagramanyan, V.P. Nerubatskiy, Int. J. Refract. Met. H. **89**, 336-339 (2019).

[6] C. Sun, Y. Li, Y. Wang, L. Zhu, Q. Jiang, Y. Miao, X. Chen, Ceram. Int. **40**, 12723-12728 (2014).

[7] U.S. Radloff, F. Kern, R. Gadow, J. Eur. Ceram. Soc. **38**, 4003-4013 (2018).

[8] C. Tuzemen, B. Yavas, I. Akin, O. Yucel, F. Sahin, G. Goller, J. Alloy. Compd. **781**, 433-439 (2019).

[9] I. Farias, L. Olmos, O. Jimenez, M. Flores, A. Braem, J. Vleugels, Trans. Nonferrous Met. Soc. China **29**, 1653-1664 (2019).

[10] L.M. Luo, J.B. Chen, H.Y. Chen, G.N. Luo, X.Y. Zhu, J.G. Cheng, X. Zan, Y.C. Wu, Fusion Eng. Des. **90**, 62-66 (2015).

[11] J. Zhang, L. Wang, W. Jiang, L. Chen, Mat. Sci. Eng. A. **487**, 137-143 (2008).

[12] H. Istgaldi, M.S. Asl, P. Shahi, B. Nayebi, Z. Ahmadi, Ceram. Int. (2019) DOI:10.1016/j.ceramint.2019.09.287

[13] A.S. Namini, Z. Ahmadi, A. Babapoor, M. Shokouhimehr, M.S. Asl, Ceram. Int. **45**, 2153-2160 (2019).

[14] D. Chakravarthy, S. Roy, P.K. Das, Bull. Mater. Sci. **28**, 3, 227-231 (2005).

[15] L. Wang, X. Shu, X. Lu, Y. Wu, Y. Ding, S. Zhang, Mater. Lett. **196**, 403-405 (2017).

[16] L. Cheng, Z. Xie, G. Liu, W. Liu, W. Xue, J. Eur. Ceram. Soc. **32**, 3399-3406 (2012).

[17] N. Shanbhog, K. Vasanthakumar, N. Arunachalam, S.R. Bakshi, Int. J. Refract. Met. H. **84**, 104979-104988 (2019).

[18] B.L. Madej, D. Garbiec, M. Madej, Vacuum. **164**, 250-255 (2019).

[19] Y.F. Zhou, Z.Y. Zhao, X.Y. Tan, L.M. Luo, Y. Xu, X. Zan, Q. Xu, K. Tokunaga, X.Y. Zhu, Y.C. Wu, Int. J. Refract. Met. H. **79**, 95-101 (2019).

[20] P. Zhanga, C. Chena, Z. Chena, C. Shena, P. Fenga, Vacuum **164**, 286-292 (2019).

[21] C. Luo, Y. Wang, J. Xu, G. Xu, Z. Yan, J. Li, H. Li, H. Lu, J. Suo, Int. J. Refract. Met. H. **81**, 27-35 (2019).

[22] B.B. Bokhonov, M.A. Korchagin, A.V. Ukhina, D.V. Dudinaa, Vacuum, **157**, 210-215 (2018).

[23] A. Teber, F. Schoenstein, F. Tetard, M. Abdellaoui, N. Jouini, Int. J. Refract. Met. H. **30**, 64-70 (2012).

[24] M. Demuynck, J.P. Erauw, O.V. Biest, F. Delannay, F. Cambier, J. Eur. Ceram. Soc. **32**, 1957-1964 (2012).

[25] Y.W. Kim, J.G. Lee, J. Am. Ceram. Soc. **12**, 1333-37 (1989).

[26] R.A. Cutler, A.C. Hurford, Mat. Sci. Eng. A., **105/106**, 183-192 (1988).

[27] J.H. Zhang, T.C. Lee, W.S. Lau, J. Mater. Process. Tech. **63**, 908-912 (1997).

[28] Z. Fu, R. Koc, Ceram. Int. **43**, 17233-17237 (2017).

[29] R. Kumar, A.K. Chaubey, S. Bathula, K.G. Prashanth, A. Dhar, J. Mater. Eng. Perform. *27*, 997-1004 (2018).

[30] O. Guillon, J.G. Julian, B. Dargatz, T. Kessel, G. Schierning, J. Rathel, M. Herrmann. Adv. Eng. Mater. **16**, 830-849 (2014).

[31] D. Zhang, L. Ye, D. Wang, Y. Tang, S. Mustapha, Y. Chen, Composites: Part A. **43**, 1587-1598 (2012).

[32] T. Fujii, K. Tohgo, P.B. Putra, Y. Shimamura, J. Mech. Behav. Biomed. **19**, 45-53 (2019).

[33] T. Thomas, C. Zhang, A. Sahu, P. Nautiyal, A. Loganathan, T. Laha, B. Boel, A. Agarwal, Mat. Sci. Eng. A. **728**, 45-53 (2018).

[34] L.K. Singh, A. Bhadauria, T. Laha, J. Mater. Res. Technol. **8**, 503-512 (2019).

[35] T. Fujii, K. Tohgo, M. Iwao, Y. Shimamura, J. Alloy. Compd. **744**, 759-768 (2018).

[36] S. Xiang, S. Ren, Y. Liang, X. Zhang, Mat. Sci. Eng. A. **768**, 138459 (2019).

[37] M.R. Akbarpour, S. Alipour, Ceram. Int. **43**, 13364-13370 (2017).

[38] W.R. Ilaham, L.K. Singh, T. Laha, Fusion Eng. Des. **138**, 303-312 (2019).

[39] U. Sabu, B. Majumdar, Bhaskar P. Saha & D. Das, Trans. Ind. Ceram. Soc. **77**, 1-7 (2018)

[40] L. Zhang, R.V. Koka, Mater. Chem. Phys. **57**, 23-32 (1998).

[41] J. Langer, M.J. Hoffmann, O. Guillon, Acta. Mater. **57**, 5454-5465 (2009).

[42] A. Babapoor, M.S. Asl, Z. Ahmadi, A.S. Namini, Ceram. Int. **44**, 14541-14546 (2018).

[43] F. Balima, A. Largeteau, Scr. Mater. **158**, 20-23 (2019).

[44] W.H. Lee, J.G. Seong, Y.H. Yoon, C.H. Jeong, C.J.V. Tyne, H.G. Lee, S.Y. Chang, Ceram. Int. **45**, 8108-8114 (2019).